Applied Catalysis B: Environmental 119–120 (2012) 13–19

Contents lists available at SciVerse ScienceDirect

Applied Catalysis B: Environmental

journal homepage: www.elsevier.com/locate/apcatb

Ultra-deep desulfurization via reactive adsorption on Ni/ZnO: The effect of ZnO particle size on the adsorption performance

Yuliang Zhang[a,b], Yongxing Yang[a], Hongxian Han[a], Min Yang[a], Lu Wang[a], Yongna Zhang[a], Zongxuan Jiang[a,**], Can Li[a,*]

[a] State Key Laboratory of Catalysis, Dalian Institute of Chemical Physics, Chinese Academy of Sciences, 457 Zhongshan Road, Dalian 116023, China
[b] Graduate University of Chinese Academy of Sciences, Beijing 100049, China

ARTICLE INFO

Article history:
Received 5 November 2011
Received in revised form 30 January 2012
Accepted 2 February 2012
Available online 10 February 2012

Keywords:
Adsorptive desulfurization
Ni/ZnO adsorbent
Size effect

ABSTRACT

The effect of ZnO particle size on the adsorptive desulfurization performance for Ni/ZnO (5 wt% NiO) adsorbent was investigated using thiophene as a sulfur containing compound in model gasoline with a fixed bed reactor. The Ni/ZnO adsorbents with different ZnO particle sizes (8, 12, 20, 30 nm) were prepared by an impregnation method and characterized by powder X-ray diffraction (XRD), high resolution transmission electron microscopy (HRTEM) and transmission electron microscopy (TEM). It was found that the adsorption capacity of the Ni/ZnO adsorbent for thiophene significantly increased with the decrease of the ZnO particle sizes. Typically at a breakthrough sulfur level of 1 mg/L, sulfur capacity of Ni/ZnO (8 nm) from model gasoline (500 mg/L) is much higher than that of Ni/ZnO (30 nm) from 84 mg sulfur per gram adsorbent to nearly 0 mg sulfur per gram adsorbent. This higher desulfurization activity and sulfur capacity for Ni/ZnO with smaller ZnO particle sizes could be derived from higher Ni dispersion on ZnO and lower mass transfer limitations of sulfur to ZnO from Ni in H_2.

1. Introduction

SO_x produced from the burning of organic sulfur-containing compounds presented in fuel oils cannot only cause acid rain, pollute air, and harm human health, but also irreversibly poison the three-way catalysts in the tail gas cleanup systems of mobile vehicles. More stringent environmental regulations have been enacted for the oil refining industries all over the world. Sulfur content in gasoline is required to be less than 10 ppm in Euro V emission limitation. However, it is difficult for conventional hydrodesulfurization (HDS) to reduce the sulfur of liquid fuels to a very low level for gasoline without loss of octane number. Therefore, new strategies for desulfurization have been exploring to meet the urgent needs to produce cleaner gasoline [1–7]. Adsorptive desulfurization (ADS) is one of the most promising complementary and alternative ways. Supported noble, transition metals and metal oxides, binary, ternary metal oxides, activated carbons, zeolites, supported polymers and many other materials have been investigated for adsorptive desulfurization [8–11]. Among these types of adsorbents explored, Ni-based adsorbent exhibited better performance for removing thiophenic sulfur compounds from liquid fuels. Song and co-workers used a nickel-based Ni–Al adsorbent in an adsorption desulfurization system at a temperature range of 25–200 °C under ambient pressure without using H_2 [12]. The nickel-based adsorbents show high selectivity and sulfur adsorption capacity for the real gasoline. Landau et al. reported adsorptive desulfurization of commercial low-sulfur (22 ppm) containing gasoline on Ni/Al–SiO_2 in a fixed bed at 230 °C [13]. They found that addition of ethanol could strongly improve the performance of reduced Ni/Al–SiO_2 adsorbents. Landau et al. attributed this effect to the catalytic dehydrogenation of EtOH generating an equimolar $CO/H_2/CH_4$ gas mixture. The presence of hydrogen alters the adsorption mode of S-organic compounds at the surface of nickel nano-particles from chemisorption to the fast reactive adsorption mode by the formation of bulk Ni_2S_2 and Ni_3S_4 phases.

The Conoco Phillips Petroleum Company developed a so-called S-Zorb process for the production of low sulfur gasoline by reactive adsorption of sulfur compounds using a solid sorbent [14–19]. The process was carried out over a fluidized-bed reactor in a temperature range between 377 and 502 °C under H_2 pressures in the range of 0.344–3.44 MPa. This process is able to preserve octane number well while removing sulfur species effectively. For the adsorbents of S-Zorb technology, Ni/ZnO was found to be the effective adsorbent for removing sulfur species. Ni functions as hydrodesulfurization sites, while ZnO takes up the resulting H_2S and is converted into ZnS simultaneously [20]. Bezverkhyy and co-workers have done

* Corresponding author. Tel.: +86 411 84379070; fax: +86 411 84694447.
** Corresponding author.
E-mail addresses: zxjiang@dicp.ac.cn (Z. Jiang), canli@dicp.ac.cn (C. Li).
URL: http://www.canli.dicp.ac.cn (C. Li).

0926-3373/$ – see front matter © 2012 Elsevier B.V. All rights reserved.
doi:10.1016/j.apcatb.2012.02.004

a series of adsorptive desulfurization experiments on the nickel-based adsorbents [21–24]. They found that the initial limiting step is the thiophene decomposition on metallic Ni of Ni/ZnO adsorbent; whereas after partial sulfidation, the thiophene diffusion becomes the rate determining step. It is well known that smaller particle size will increase the rate of sulfur transfer in ZnO adsorbent, especially in the latter desulfurization process of thiophene diffusion. Zhang et al. studied the influences of ZnO textural properties on the desulfurization activity of the corresponding Ni/ZnO adsorbents, and they found that ZnO with larger surface area and smaller crystal particles resulted in better desulfurization activity [19]. However, the mechanism of desulfurization by reactive adsorption via Ni/ZnO with different ZnO particle sizes has not been well understood. It is not clear how the particle size of ZnO influences the desulfurization activity and the adsorption capacity. And it should also note that more than 10 wt% of nickel loading was generally required in order to ensure the desulfurization activity of adsorbent [13,18]. Smaller particle size of ZnO might also lead to less amount of Ni loading while retaining the desulfurization activity. These issues motivated us to study the effect of ZnO particle size on the adsorption performance of Ni/ZnO for ultra-deep desulfurization.

In this work, ZnO samples with different particle sizes and Ni/ZnO adsorbents with 5 wt% NiO loading were prepared and characterized by XRD, TEM and HRTEM. To evaluate the ADS activity of the Ni/ZnO adsorbents, a series of adsorptive desulfurization (ADS) experiments were performed using a fixed-bed reactor. It was found that the Ni/ZnO loaded with smaller ZnO particle could remove sulfur more efficiently compared to that loaded with larger ZnO particle size. As expected, the apparent activation energy of Ni/ZnO loaded with smaller ZnO particle size is much lower than that loaded with larger ZnO particle size.

2. Experimental

2.1. Preparation of adsorbents

$Ni(NO_3)_2{\cdot}6H_2O$, $Zn(CH_3COO)_2{\cdot}2H_2O$, NaOH and iso-Propyl alcohol (*i*-PrOH, analytical grade) were purchased from Kermal. Polyvinylpyrrolidone (PVP, analytical grade) was purchased from Sinopharm. The adsorbents were prepared by two steps method. Firstly, ZnO samples with different particle sizes were prepared [25]. Zinc acetate (15.0 mmol) was dissolved in 1000 ml of *i*-propanol under vigorous stirring at 50 °C and quenched in ice bath. After addition of PVP, the reaction mixture was kept stirring for ca. 12 h. The hydrolyzation was performed by the addition of NaOH solution in *i*-PrOH (37.5 mmol in 500 ml) under ultrasonic agitation for ca. 2 h. The solvents were then removed by rotavaporization. The resulting mixture was washed with water to give precipitation of white ZnO nanocrystals. The ZnO precipitate was centrifuged and dried in a vacuum for 10 h (denoted as as-prepared ZnO). Three batches of such prepared ZnO samples were further calcined at 350, 400, 500 and 650 °C to obtain calcined ZnO samples with different particle sizes. Ni was supported on ZnO by incipient wetness impregnation method (IM) using $Ni(NO_3)_2$ solution as Ni precursor. The 5 wt% NiO/ZnO sample was prepared by calcination of $Ni(NO_3)_2$/ZnO at 300 °C (the NiO loading in NiO/ZnO adsorbents hereafter are 5 wt% if there is no specific notification). The ZnO nanocrystal with the size of x nm was denoted as ZnO-*x* and so it is for Ni/ZnO-*x*, which is prepared from ZnO-*x* accordingly. The 10 wt% NiO/ZnO-*x* and 15 wt% NiO/ZnO-*x* adsorbents were also prepared in the same way. The NiO/ZnO would be in situ reduced to Ni/ZnO in a fixed bed reactor before adsorptive desulfurization process.

2.2. Characterization of adsorbents

XRD patterns were recorded on a Rigaku MiniFlex diffractometer with a Cu Kα radiation source and operating at V = 40 kV and I = 200 mA. Diffraction patterns were collected from 20° to 75° at a speed of 5°/min.

Transmission electron microscopy (TEM) (FEI Tecnai G2 spirit) was used to characterize the as-prepared ZnO and the Ni/ZnO adsorbents at an accelerating voltage of 120 kV. HRTEM micrographs were obtained using a FEI Tecnai G2 F30 S-Twin microscope equipped with EDAX operating at an accelerating voltage of 300 kV. The samples for HRTEM were prepared by depositing a drop of ultrasonicated ethanol suspension of solid catalyst on the copper grid.

BET surface areas were measured on a Nova 4200e apparatus by N_2 adsorption at 77 K. The specific surface areas were calculated by BET method.

2.3. Evaluation of ADS performance of Ni/ZnO

The adsorption experiments were performed at a fixed-bed reactor at the temperature in the range between 250 and 300 °C and under operating conditions, i.e., H_2 partial pressure of 0.4 MPa, LHSV of 6 h^{-1}, and H_2/Oil of 600 NL/L. The feedstock of model gasoline is n-heptane containing thiophene with the total sulfur concentration of 500 mg/L. All of the sulfur contents reported in this work were determined by an Antek 9000S total sulfur analyzer.

In Figs. 3–8, the vertical axis stands for the transient sulfur removal (Sulfur removal), the horizontal axis stands for the cumulative effluent volume (effluent) (ml) normalized by the total adsorbent weight (g). The Sulfur removal and Effluent were expressed as Eqs. (1) and (2) respectively, where C_0 is the sulfur concentration in the feed (mg/L), C_t is the transient effluent sulfur concentration (mg/L) at any time t (min), ν is the feed volumetric flow rate (ml/min), and $m_{adsorbent}$ is the weight of the adsorbent (g).

$$\text{Sulfur removal} = \left(1 - \frac{C_t}{C_0}\right) \times 100\% \quad (1)$$

$$\text{Effluent} = \frac{\nu t}{m_{adsorbent}} \quad (2)$$

The adsorption amounts (normalized per adsorbent weight) were obtained after solving the following Eq. (3) [26].

$$q_{ad} = \frac{\nu}{1000 \times m_{adsorbent}} \int_0^t (C_0 - C_t)dt \quad (3)$$

where q_{ad} is the total amount of sulfur adsorbed (mg/g).

3. Results and discussion

3.1. Characterization of nano-sized Ni/ZnO

The powder-XRD patterns (Fig. 1) show that the prepared ZnO samples were wurtzite ZnO. Based on the full width at half-maximum (fwhm) of the highest intensity peak of ZnO (1 0 1) peak, the average particle sizes of ZnO samples were estimated by the Debye–Scherrer formula. The calculated results show that the average particle size of as-prepared ZnO nano-particles and those calcined at the temperatures of 350 °C, 400 °C, 500 °C and 650 °C are 8, 12, 20, 30 and 70 nm, respectively. This is consistent with the broadening of the diffraction peaks with decrease of the particle sizes as observed in the XRD patterns.

Fig. 2 displays the TEM images of ZnO samples. It can be seen that the ZnO nano-particles are pseudospherical in shape. The particle size of ZnO-8 shown in TEM is consistent with that calculated from

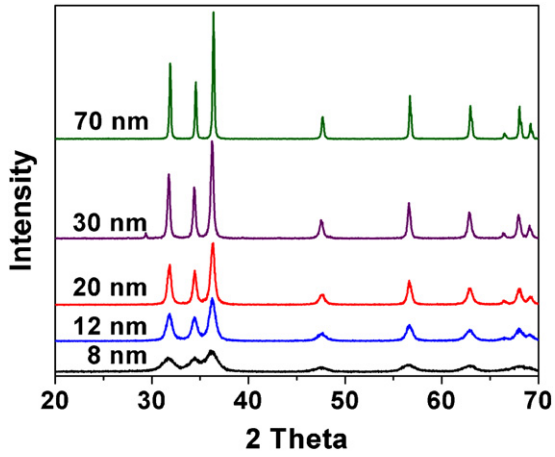

Fig. 1. The powder-XRD patterns of different ZnO samples.

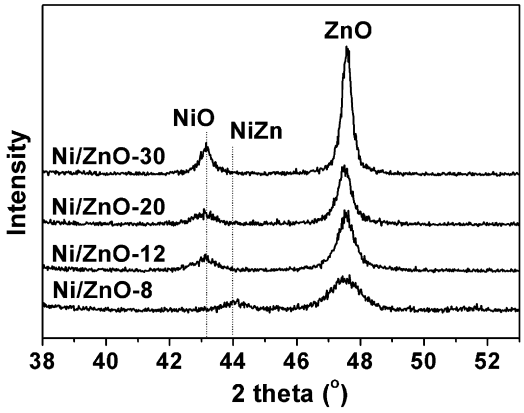

Fig. 3. The dependence of desulfurization performance on nickel amount and ZnO particle size.

the corresponding XRD pattern, while the sizes of other ZnO particles showed a little larger compared to the sizes calculated from the corresponding XRD patterns. Overall, the XRD and TEM characterization results indicate that the particle sizes of the prepared ZnO samples are in the range of 8–70 nm.

The powder XRD patterns of Ni/ZnO-*x* are shown in Fig. 3. For Ni/ZnO-12, Ni/ZnO-20 and Ni/ZnO-30 samples, the diffraction peak at $2\theta = 43.1^\circ$ can be attributed to NiO (ICDD-PDF No. 65-2901). The broadening of diffraction peak for Ni/ZnO-12 and Ni/ZnO-20 samples indicates that the NiO disperses better than NiO on Ni/ZnO-30. However, for Ni/ZnO-8, the peak appears at $2\theta = 43.9^\circ$, which can belong to the pattern of NiZn alloy (ICDD-PDF No. 65-3203). The formation of NiZn alloy could protect the Ni phase from agglomeration in the subsequent reduction treatment and desulfurization process. This may imply that the ZnO with smaller particle size of 8 nm is more active and interacts with NiO phase.

The BET surface areas of ZnO and Ni/ZnO samples with different particle sizes are summarized in Table 1. With the increase of the particle sizes of ZnO and Ni/ZnO samples, the BET surface areas were decreased.

3.2. Desulfurization performance of Ni/ZnO

Fig. 4 shows the impact of the amount of nickel loading together with ZnO particle sizes of adsorbents on the desulfurization

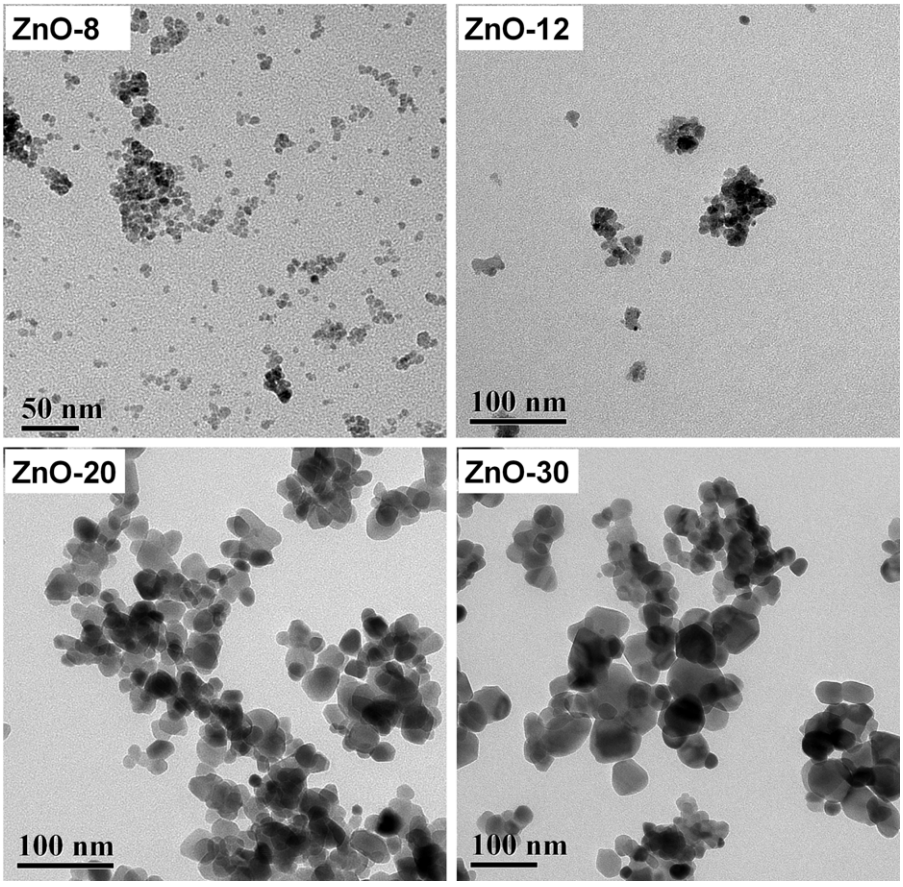

Fig. 2. TEM images of ZnO samples with different particle size.

Table 1
Specific surface area (S_{BET}) of ZnO-*x* and Ni/ZnO-*x* samples.

Sample	ZnO-8	ZnO-12	ZnO-20	ZnO-30	Ni/ZnO-8	Ni/ZnO-12	Ni/ZnO-20	Ni/ZnO-30
S_{BET} (m^2/g)	35.9	34.3	28.4	12.4	33.8	23.8	17.5	14.6

performance. Comparison of the Ni loading on the ZnO particles with the average size of 70 nm clearly shows that the ADS activity increases with the increase of the nickel loadings. However, the Ni/ZnO-30 adsorbent shows an equivalent ADS activity to that of 10 wt% Ni/ZnO-70 adsorbent, indicating that reduction of ZnO particle size can also effectively improve the desulfurization performance of Ni/ZnO adsorbents.

In order to further understand how the particle size of ZnO improves the ADS activity of the Ni/ZnO, the ADS properties of all of the four Ni/ZnO-*x* adsorbents were evaluated with reactive adsorption experiments and the results are given in Fig. 5. The Ni/ZnO-30 adsorbent has sulfur removal of 45.7% at effluent of 72 ml, though the sulfur removal at the initial desulfurization stage is slightly higher (ca. 63%). When the size of ZnO is reduced to 20 nm, the sulfur removal of the adsorbent had increased to ca. 70%. For the Ni/ZnO-12 adsorbent, the removal of sulfur-containing compounds maintains over 90% for more than 70 ml model gasoline. The Ni/ZnO-8 adsorbent has the best desulfurization performance. The sulfur concentration in model gasoline treated by the Ni/ZnO-8 adsorbent was less than 1 mg/L in the investigated region,

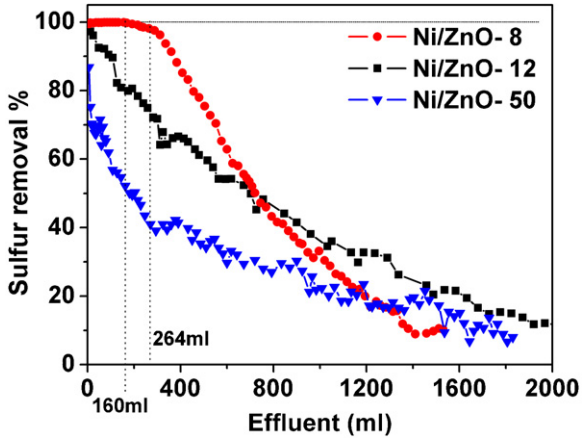

Fig. 6. Breakthrough curves for the adsorptive desulfurization of model gasoline on Ni/ZnO-8, Ni/ZnO-12 and Ni/ZnO-50 at 300 °C (the outlet sulfur content of model gasoline treated by Ni/ZnO-8 adsorbent: 160 ml with below 1 mg/L and 264 ml with below 10 mg/L).

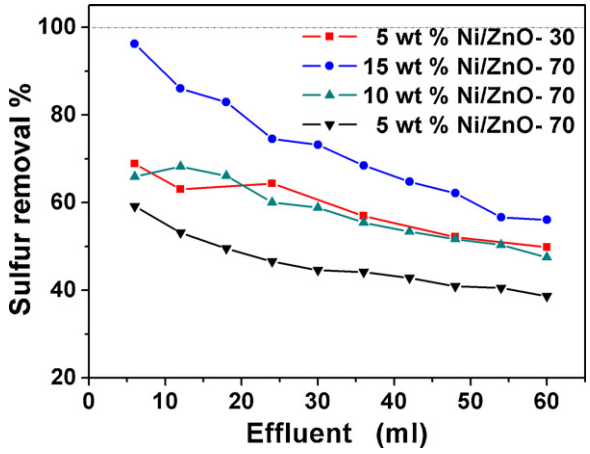

Fig. 4. The powder-XRD patterns of different Ni/ZnO-*x* samples.

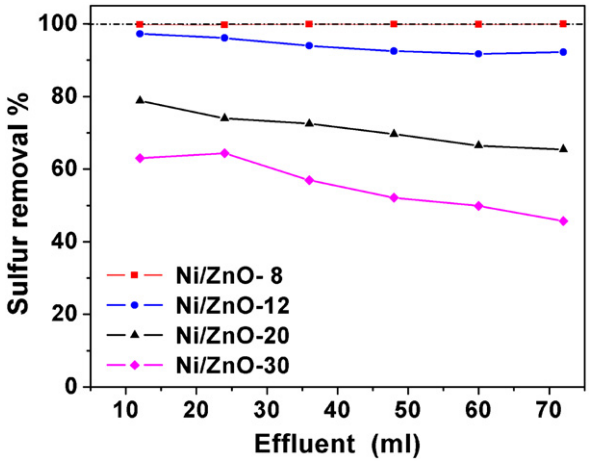

Fig. 5. The effect of ZnO particle sizes on desulfurization performance of Ni/ZnO for model gasoline at 300 °C.

indicating that nearly all sulfur in model gasoline was removed. It can be concluded that the desulfurization activity of adsorbents is related with the particle size of the ZnO. As the particle size of the ZnO reduced, the ADS activity of Ni/ZnO increases greatly. In particular, the Ni/ZnO-8 adsorbent can remove sulfur to less than 1 mg/L. For the reactive ADS process via Ni/ZnO adsorbent, the first step is thiophene decomposition on Ni and formation of NiS [20,22,23]. Then NiS will be regenerated by ZnO with the assistance of H_2. The smaller particle size of ZnO leads to higher dispersion of the metallic Ni component with smaller Ni particle sizes. This results in better catalytic activity for thiophene activation and decomposition, which leads to high ADS activity.

In order to evaluate the sulfur adsorption capacity of the Ni/ZnO-8 adsorbent, a breakthrough experiment was performed. Fig. 6 shows the breakthrough curve for the adsorptive removal of thiophene over Ni/ZnO-8 adsorbent. From the curve we can see that more than 160 ml model gasoline with sulfur content below 1 mg/L can be obtained, corresponding to a breakthrough sulfur capacity of 84 mg/g of the adsorbent (mg/g adsorbent). In addition, the breakthrough capacity of the Ni/ZnO-8 adsorbent at an outlet sulfur level of 10 mg/L is about 131 mg/g adsorbent, corresponding to 264 ml of effluent. However, the desulfurization property of Ni/ZnO-12 adsorbent decreased sharply in the long run experiment. The difference might be explained by the conclusion of Fig. 3. For Ni/ZnO-8 sample, the XRD diffraction pattern shows that the NiZn alloy has been formed in calcination, which would enhance the interaction between Ni and ZnO. We assume that the strong interaction could accelerate the transfer of sulfur from NiS to ZnO with the assistance of H_2, because the NiS and ZnS could form a compound of $NiS_{33.3}Zn_{32.3}$ (ICDD-PDF No. 65-4586). The $NiS_{33.3}Zn_{32.3}$ has a similar cubic structure to NiZn alloy, which makes the transfer of sulfur from NiS to ZnO much easier. This hypothesis is different from the assumption made by Bezverkhyy et al. [23]. They found there is a decline of desulfurization activity of reduced NiO/ZnO adsorbent in the initial period of ADS process compared to the unreduced sample and attribute it to the formation of NiZn alloy. We suppose that the decline may be due to an agglomeration of the metallic Ni in reduction treatment at high temperature. Another factor affect the

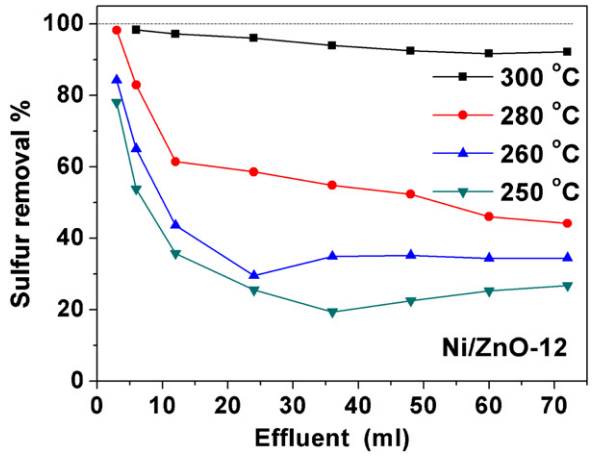

Fig. 7. Adsorptive desulfurization of model gasoline on Ni/ZnO-12 at different adsorption temperature.

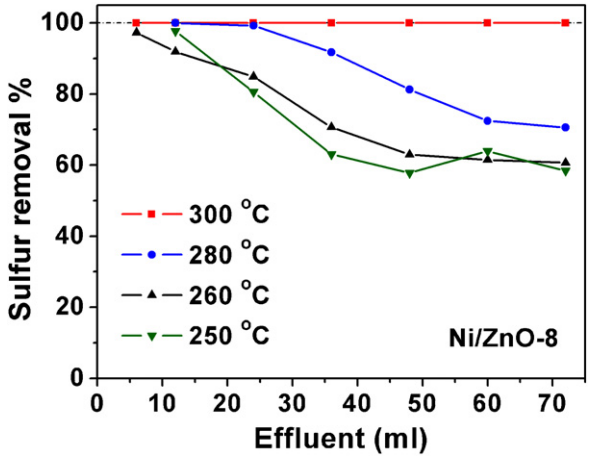

Fig. 8. Adsorptive desulfurization of model gasoline on Ni/ZnO-8 at different temperature.

desulfurization activity is the diffusion path. The Ni/ZnO-8 adsorbent has a shorter diffusion distance than that of Ni/ZnO-12 when the ZnO was partially sulfided. Furthermore, after calculation from the breakthrough curve, we found that the total sulfur capacities of the Ni/ZnO-8 and Ni/ZnO-12 adsorbents are 406.2 and 412.2 mg/g respectively, approximately equal to its theoretical capacity of 394.9 mg/g. This indicates that ZnO of the Ni/ZnO-8 and Ni/ZnO-12 adsorbents could be completely transformed to ZnS. Here, the practical adsorptive capacity slightly exceeds the theoretical capacity, which can be understood well if one considers the additional contribution from the ADS activity of NiS/ZnS in the end of breakthrough experiment, which was also taken into account during the practical total capacity calculation. The Ni/ZnO prepared using commercial ZnO with average particle size of 50 nm presents unsatisfying desulfurization result. The initial sulfur removal quickly dropped to 70% and the total capacity of the Ni/ZnO-50 adsorbent is 260.5 mg/g, corresponding to ZnO consumption ratio of only 66%. This indicates that the kernel ZnO of big ZnO particle is very difficult to transform into ZnS. On the contrary, the Ni/ZnO-8 adsorbent has a low adsorption mass transfer zone, demonstrating lower resistance to mass transfer. This is in good accordance with the former conclusion. In conclusion, for the adsorbent of Ni/ZnO-8, the interaction between metallic Ni and ZnO enhanced by NiZn alloy and the small radius of particle size could reduce the resistance in S transfer from NiS to ZnO. Consequently, the Ni/ZnO-8 not only shows its excellent desulfurization activity at the start of run, but also keeps the high activity even when the ZnO is partially sulfide. As a result, the Ni/ZnO-8 adsorbent improves the sulfur removal and the adsorption capacity.

3.3. *Effect of temperature on desulfurization of model gasoline on Ni/ZnO*

We investigated the effect of temperature on desulfurization performance of model gasoline over Ni/ZnO adsorbents and the result is displayed in Figs. 7 and 8. The removal of thiophene over Ni/ZnO-12 adsorbent at 300 °C is 90% (Fig. 7). When the temperature decreased to 280 °C, the thiophene conversion dropped dramatically to 50%. The desulfurization activity continued to decline as the temperature decreased. In Fig. 8, we observed that the reaction of Ni/ZnO-8 adsorbent with thiophene has similar results at various reaction temperatures. The removal of thiophene is still very high at 280 °C (70%), which is higher than that over Ni/ZnO-12 by 20%. In addition, the desulfurization property of Ni/ZnO-8 is less affected by temperature than that of Ni/ZnO-12. To further understand such phenomenon, the desulfurization activity of Ni/ZnO-8 adsorbent at 280 °C is compared with those of Ni/ZnO-20 and Ni/ZnO-30 at 300 °C. It can be seen that the desulfurization profiles of Ni/ZnO-8 adsorbent at 280 °C is still the best one, despite the other two adsorbents removing sulfur at a high temperature. In Ni/ZnO system, ZnO acts as a sulfur accepter, accepting diffused H_2S from thiophene decomposition on Ni.

It is proposed that the nano-ZnO with smaller particle size could lead to better dispersion of Ni on the ZnO surface, providing more active sites for thiophene decomposition in H_2. Moreover, it can also imagine that the surface of smaller nano-ZnO has high free energy, leading to readily react with H_2S [23].

3.4. *The kinetic study of desulfurization on Ni/ZnO with different particle sizes*

To have a more detailed look at the behavior of particle size on ADS of Ni/ZnO adsorbents, we investigated the kinetic activity of desulfurization on Ni/ZnO adsorbents. The reactive adsorptive desulfurization process was treated as a pseudo first order reaction, and Eq. (4) was used in order to evaluate the apparent reaction rate constant. Then an approximate linear relationship was obtained for the thiophene component.

$$k = -\mathrm{LHSV}\ \ln\left(\frac{C_t}{C_0}\right) + C_1 \tag{4}$$

$$\ln k = -\frac{E_a}{RT} + C_2 \tag{5}$$

where k is the apparent reaction rate constant, C_1 is a constant. The dependence of $\ln k$ on inverse temperature gives an Arrhenius type plot (Eq. (5)) from which the apparent activation energy (E_a) of the reaction can be calculated (Fig. 9). Calculated apparent activation energy data are displayed in Fig. 9. It can be seen that the apparent activation energy of thiophene on these adsorbents decreases in the following order: Ni/ZnO-30 > Ni/ZnO-20 > Ni/ZnO-12 > Ni/ZnO-8. It is in good accordance with the desulfurization performance of these adsorbents showed in Fig. 5. The apparent activation energy of Ni/ZnO-8 (32 kJ/mol) is only nearly 40% of that of Ni/ZnO-30 adsorbent (80 kJ/mol), which indicates that there might be some differences in the adsorbent structures between Ni/ZnO-8 and Ni/ZnO-30. HRTEM image provides a finer structure of Ni/ZnO-8 adsorbent (Fig. 10a). Because Ni/ZnO adsorbent in the ADS experiment is produced from NiO/ZnO by in situ H_2 reduction, here in HRTEM characterization, NiO/ZnO is selected to be studied. In this HRTEM image, both the surface and the bulk of the adsorbent particles barely exhibit the lattice fringe of ZnO (e.g. a basal spacing of 2.48 Å, according to ZnO (1 0 1) lattice planes). We could not

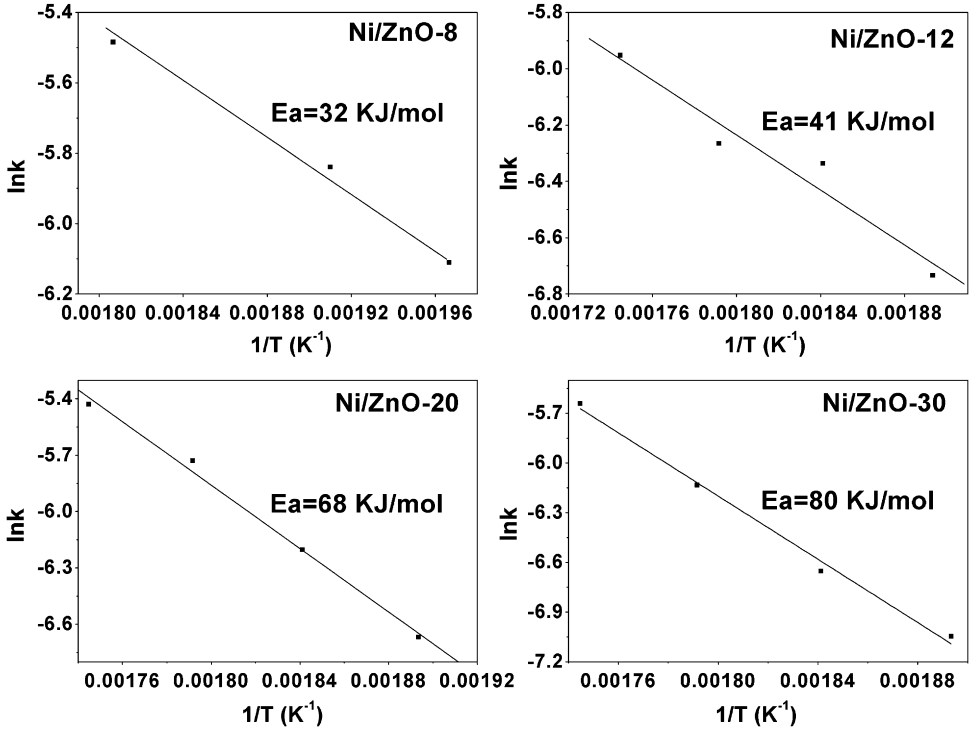

Fig. 9. Arrhenius apparent activation energies for different Ni/ZnO adsorbents.

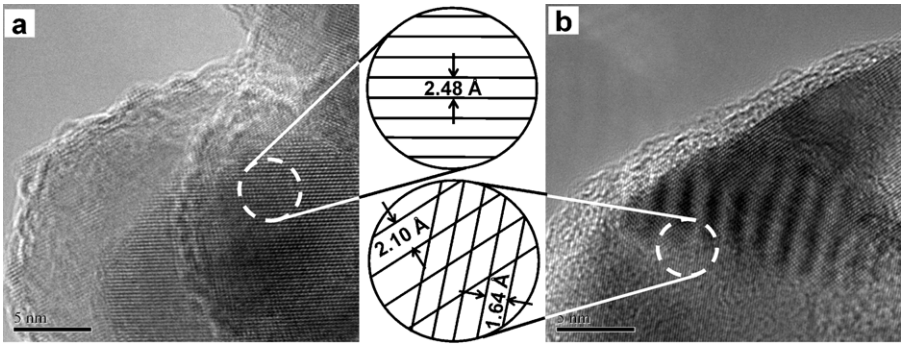

Fig. 10. HRTEM images of adsorbents Ni/ZnO-8 (a) and Ni/ZnO-30 (b).

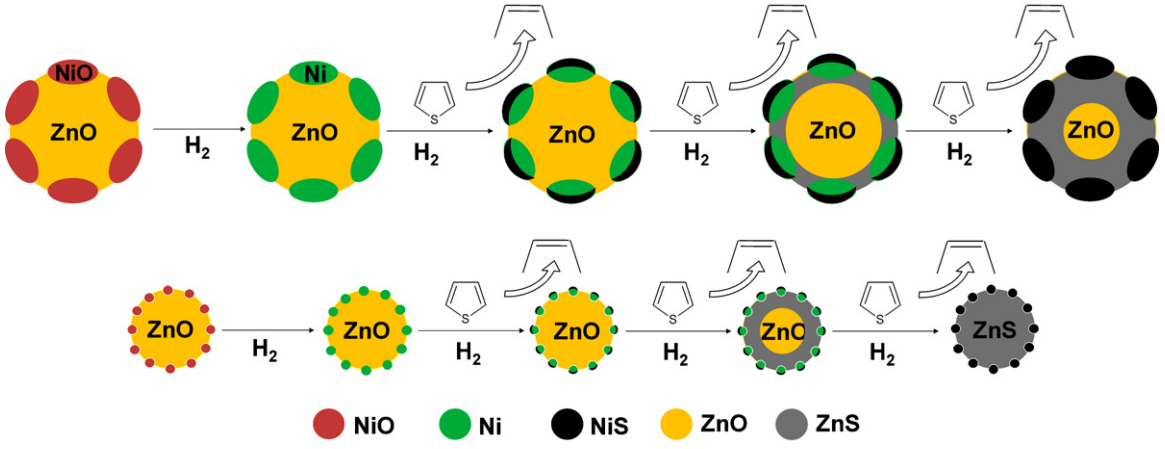

Scheme 1. Proposed scheme for the desulfurization process over Ni/ZnO with different ZnO particle sizes.

find the basal spacing assigned to NiO (2 0 0) lattice planes (2.09 Å). However, the EDX characterization shows obviously K peak of Ni. It demonstrates that the NiO phase was highly dispersed on the ZnO particles, as evidenced by the weaker lattice fringe of NiO almost completely covered by that of ZnO. This high dispersion of the Ni on ZnO could promote the auto-regeneration of NiS to metallic Ni, explaining why the NiO/ZnO-8 has so excellent sulfur removal activity. Fig. 10b presents the lattice fringes of NiO (2 0 0) with a spacing of 2.1 Å and ZnO (1 1 0) with a spacing of 1.64 Å on NiO/ZnO-30. The appearance of NiO (2 0 0) shows an aggregation of NiO. This indicates the low dispersion of NiO exists on NiO/ZnO-30 and there will be less NiO explored on the ZnO particles. This phenomenon results in a low ADS activity of NiO/ZnO-30.

Since the sulfur diffusion becomes a rate determining step when the ZnO is partially sulfided, the particle size of ZnO greatly affects the performance in the long time run of ADS. Scheme 1 describes a proposed desulfurization process over Ni/ZnO with different particle sizes. For the ZnO with smaller particle sizes, the NiO could highly disperse on the ZnO surface so that the adsorbent show a higher initial desulfurization property. After the shell of the ZnO particle was sulfided, the smaller particle size of ZnO could effectively decrease the mass transfer difficulty of sulfur diffusion in ZnO, leading to a high sulfur removal in latter desulfurization stage. For this reason, the Ni/ZnO adsorbent from ZnO precursor with smaller particle sizes could maintain its super high ADS activity and results in a much higher adsorption capacity. On the contrary, it is difficult for H_2S to react with the core part of the bigger ZnO particles and the adsorbent has a lower adsorption capacity quite deservedly.

4. Conclusions

We prepared Ni/ZnO adsorbents from nano-ZnO precursor with different particle sizes. The desulfurization performance of the adsorbents strongly depends on the particle sizes of ZnO. As the grain of ZnO diminishes, both the desulfurization activity and sulfur capacity of the Ni/ZnO adsorbents enhance gradually. The Ni/ZnO-8 shows an excellent desulfurization performance, which achieves a breakthrough capacity of 84 mg/g of the adsorbent (mg/g) with sulfur content of effluent below 1 mg/L, which is much higher than that of Ni/NiO-30 near to 0 mg/g adsorbent. The XRD and HRTEM characterization shows that the smaller ZnO particle size promotes the dispersion of NiO on ZnO support and metallic Ni and ZnO will directly form NiZn alloy in calcination when the particle size of ZnO smaller than 8 nm. This interaction of the Ni and ZnO could prevent Ni phase from agglomeration and help the sulfur atom transfer from Ni phase to ZnO through a $NiS_{33.3}Zn_{32.3}$ structure. The adsorbent Ni/ZnO-8 has very low apparent activation energy of 32 kJ/mol, much lower than that for Ni/ZnO-30 adsorbent (80 kJ/mol).

Acknowledgment

This work was supported by National Nature Science Foundation of China (NSFC grant no. 21173214, NSFC grant no. 20973163) and the State Key Project of China (no. 2006CB202506).

References

[1] I.V. Babich, J.A. Moulijn, Fuel 82 (2003) 607–631.
[2] C.S. Song, Catal. Today 86 (2003) 211–263.
[3] X.L. Ma, L. Sun, C.S. Song, Catal. Today 77 (2002) 107–116.
[4] C. Li, Z.X. Jiang, J.B. Gao, Y.X. Yang, S.J. Wang, F.P. Tian, F.X. Sun, X.P. Sun, P.L. Ying, C.R. Han, Chem. Eur. J. 10 (2004) 2277–2280.
[5] R.T. Yang, A.J. Hernandez-Maldonado, F.H. Yang, Science 301 (2003) 79–81.
[6] R. Prins, A. Egorova, A. Rothlisberger, Y. Zhao, N. Sivasankar, P. Kukula, Catal. Today 111 (2006) 84–93.
[7] X. Li, F. Zhou, A.J. Wang, L.Y. Wang, Y.K. Hu, Ind. Eng. Chem. Res. 48 (2009) 2870–2877.
[8] E.O. Sako, H. Kondoh, I. Nakai, A. Nambu, T. Nakamura, T. Ohta, Chem. Phys. Lett. 413 (2005) 267–271.
[9] Z.X. Jiang, Y. Liu, X.P. Sun, F.P. Tian, F.X. Sun, C.H. Liang, W.S. You, C.R. Han, C. Li, Langmuir 19 (2003) 731–736.
[10] Y.X. Yang, H.Y. Lu, P.L. Ying, Z.X. Jiang, C. Li, Carbon 45 (2007) 3042–3044.
[11] Y.H. Wang, F.H. Yang, R.T. Yang, J.M. Heinzel, A.D. Nickens, Ind. Eng. Chem. Res. 45 (2006) 7649–7655.
[12] X.L. Ma, M. Sprague, C.S. Song, Ind. Eng. Chem. Res. 44 (2005) 5768–5775.
[13] M.V. Landau, M. Herskowitz, R. Agnihotri, J.E. Kegerreis, Ind. Eng. Chem. Res. 47 (2008) 6904–6916.
[14] K. Tawara, T. Nishimura, H. Iwanami, T. Nishimoto, T. Hasuike, Ind. Eng. Chem. Res. 40 (2001) 2367–2370.
[15] G.P. Khare, G.J. Greenwood, Abstr. Pap. Am. Chem. Soc. 218 (1999), U615–U615.
[16] G.P. Khare, G.A. Delzer, D.H. Kubicek, G.J. Greenwood, Environ. Prog. 14 (1995) 146–150.
[17] G.P. Khare, D.R. Engelbert, B.W. Cass, US Patent 5914292 (1999).
[18] G.P. Khare, D.R. Engelbert, B.W. Cass, US Patent 6056871 (2000).
[19] J.C. Zhang, Y.Q. Liu, S.A. Tian, Y.M. Chai, C.G. Liu, J. Nat. Gas Chem. 19 (2010) 327–332.
[20] K. Tawara, T. Nishimura, I. Iwanami, Sekiyu Gakkaishi 43 (2000) 114–120.
[21] I. Bezverkhyy, G. Gadacz, J.P. Bellat, Mater. Chem. Phys. 114 (2009) 897–901.
[22] I. Bezverkhyy, A. Ryzhikov, G. Gadacz, J.P. Bellat, Catal. Today 130 (2008) 199–205.
[23] A. Ryzhikov, I. Bezverkhyy, J.P. Bellat, Appl. Catal. B: Environ. 84 (2008) 766–772.
[24] I. Bezverkhyy, O.V. Safonova, P. Afanasiev, J.P. Bellat, J. Phys. Chem. C 113 (2009) 17064–17069.
[25] L. Guo, S.H. Yang, C.L. Yang, P. Yu, J.N. Wang, W.K. Ge, G.K.L. Wong, Chem. Mater. 12 (2000) 2268–2274.
[26] A.J. Hernandez-Maldonado, R.T. Yang, Ind. Eng. Chem. Res. 43 (2004) 1081–1089.